Synthesis, Structure, and Characterization of a New Second-Harmonic-Generating Tellurite: $Na_2TeW_2O_9$

Joanna Goodey, Jake Broussard, and P. Shiv Halasyamani*

Department of Chemistry, University of Houston, 4800 Calhoun Boulevard, Houston, Texas 77204-5003

Received February 25, 2002. Revised Manuscript Received April 24, 2002

The synthesis, structure, and characterization of a new noncentrosymmetric tellurite, $Na_2TeW_2O_9$, is reported. The oxide exhibits a three-dimensional structure comprising distorted $W^{6+}O_6$ octahedra linked to asymmetric $Te^{4+}O_3$ groups. Both cations are in local acentric environments attributable to second-order Jahn−Teller effects. Single crystals of $Na_2TeW_2O_9$ were synthesized through supercritical hydrothermal methods, utilizing $NaOH_{(aq)}$, WO_3, and TeO_2 as reagents. Polycrystalline $Na_2TeW_2O_9$ was synthesized by combining stoichiometric amounts of Na_2CO_3, WO_3, and TeO_2 through standard solid-state methods. $Na_2TeW_2O_9$ crystallizes in the noncentrosymmetric space group *Ia* (No. 9) with $a = 13.1394(5)$ Å, $b = 7.3202(3)$ Å, $c = 31.4435(11)$ Å, and $\beta = 95.0270(10)°$. Powder SHG measurements, using 1064-nm radiation, on polycrystalline $Na_2TeW_2O_9$ indicated a strong SHG intensity of approximately 500× SiO_2. Additional SHG measurements revealed the material is phase-matchable (Type I).

Introduction

One challenge currently faced by the materials community is the synthesis of compounds with efficient second-order nonlinear optical (NLO) behavior, that is, frequency doubling or second-harmonic generation (SHG).[1−5] Enhancing the SHG capability of materials relies on understanding the structure−property relationships associated with the phenomenon. One necessary structural prerequisite for SHG is crystallographic noncentrosymmetry (NCS).[6] With inorganic materials, macroscopic NCS is often a consequence of the acentric coordination of certain metal cations. This local acentricity is a necessary, but not sufficient condition for generating crystallographic NCS. In other words, the material may crystallize with the acentric units aligned in an antiparallel manner, resulting in crystallographic centrosymmetry. In a review of NCS oxides,[3] we determined the influence of a second-order Jahn−Teller (SOJT) distortion[7−13] on the NCS structure. A strategy that we have employed to create NCS materials involves synthesizing compounds that contain cations susceptible to SOJT distortions, namely, d^0 transition metals (Ti^{4+}, Nb^{5+}, or W^{6+}) and cations with nonbonded electron pairs (Se^{4+}, Te^{4+}, or Sb^{3+}).[14−18]

In addition to the crystallographic NCS requirement, viable SHG materials should also be optically transparent in the relevant wavelengths, be air- and moisture-stable, and be able to withstand laser irradiation. For inorganic compounds, oxides seem the best materials of choice, as evidenced by a number of complexes with strong SHG efficiencies, such as, $KTiOPO_4$ (KTP), $LiNbO_3$, and $BaTiO_3$. Other than crystallographic NCS, one common structural feature of highly efficient SHG materials, that is, an SHG response >400× SiO_2, is the "constructive addition" of the individual bond hyperpolarizabilities, $\beta(M^{n+}-O)$. It is this constructive addition of bond hyperpolarizabilities that is thought to be responsible for the large SHG responses found in KTP, $LiNbO_3$, and $BaTiO_3$.[19−22] We have chosen to investigate the $Na-Te^{4+}-d^0-$oxide system, specifically where the d^0 transition metal is W^{6+}, to couple the SOJT distortions of W^{6+} and Te^{4+} and thereby promote the formation of a material with a strong SHG response.

With respect to the $Na-Te^{4+}-d^0-$oxide system, a few materials have been reported.[23−26] Zero, one, two and

(1) Chen, C.; Liu, G. *Annu. Rev. Mater. Sci.* **1986**, *16*, 203.
(2) Marder, S. R.; Sohn, J. E.; Stucky, G. D. *Materials for Non-Linear Optics: Chemical Perspectives*; American Chemical Society: Washington, D.C., 1991.
(3) Halasyamani, P. S.; Poeppelmeier, K. R. *Chem. Mater.* **1998**, *10*, 2753.
(4) Becker, P. *Adv. Mater.* **1998**, *10*, 979.
(5) Keszler, D. A. *Curr. Opin. Solid State Mater. Sci.* **1999**, *4*, 155.
(6) Nye, J. F. *Physical Properties of Crystals*; Oxford University Press: Oxford, 1957.
(7) Opik, U.; Pryce, M. H. L. *Proc. R. Soc. (London)* **1957**, *A238*, 425.
(8) Bader, R. F. W. *Mol. Phys.* **1960**, *3*, 137.
(9) Bader, R. F. W. *Can. J. Chem.* **1962**, *40*, 1164.
(10) Pearson, R. G. *J. Am. Chem. Soc.* **1969**, *91*, 4947.
(11) Pearson, R. G. *J. Mol. Struct.* **1983**, *103*, 25.
(12) Wheeler, R. A.; Whangbo, M.-H.; Hughbanks, T.; Hoffmann, R.; Burdett, J. K.; Albright, T. A. *J. Am. Chem. Soc.* **1986**, *108*, 2222.
(13) Kunz, M.; Brown, I. D. *J. Solid State Chem.* **1995**, *115*, 395.
(14) Porter, Y.; Bhuvanesh, N. S. P.; Halasyamani, P. S. *Inorg. Chem.* **2001**, *1172*, 40.
(15) Porter, Y.; Ok, K. M.; Bhuvanesh, N. S. P.; Halasyamani, P. S. *Chem. Mater.* **2001**, *13*, 1910.
(16) Ok, K. M.; Bhuvanesh, N. S. P.; Halasyamani, P. S. *Inorg. Chem.* **2001**, *40*, 1978.
(17) Ok, K. M.; Bhuvanesh, N. S. P.; Halasyamani, P. S. *J. Solid State Chem.* **2001**, *161*, 57.
(18) Porter, Y.; Halasyamani, P. S. *Inorg. Chem.*, submitted.
(19) DiDomenico, M.; Wemple, S. H. *J. Appl. Phys.* **1969**, *40*, 720.
(20) Jeggo, C. R.; Boyd, G. D. *J. Appl. Phys.* **1970** *41*, 2741.
(21) Levine, B. F. *Phys. Rev. B* **1972**, *7*, 2600.
(22) Bergman, J. G.; Crane, G. R. *J. Solid State Chem.* **1975**, *12*, 172.
(23) Balraj, V.; Vidyasagar, K. *Inorg. Chem.* **1998**, *37*, 4674.

10.1021/cm020087i CCC: $22.00
Published on Web 06/11/2002

three-dimensional $A^{+}-M^{6+}-Te^{4+}-O$ (where A = Na, K, Rb, Cs, NH_4^+; M = Mo, W) phases are known. Two notable compounds are the layered quaternary tellurites $Cs_2Mo_3TeO_{12}$ and $(NH_4)_2Mo_3TeO_{12}$,[23] both of which are noncentrosymmetric. Our hydrothermal investigation of the Na−Te−W−O phase space has resulted in the synthesis of a new noncentrosymmetric tellurite, $Na_2TeW_2O_9$. The three-dimensional structure consists of corner-sharing layers of $W^{6+}O_6$ octahedra that are connected through asymmetric Te^{4+} cations. $Na_2TeW_2O_9$ exhibits a strong SHG efficiency of approximately 500× quartz and has been determined to be phase-matchable (Type I). The synthesis, structure, and characterization of this novel tellurite are presented.

Background

Typically, powder SHG measurements have been limited to reporting the SHG efficiency with respect to a standard, usually SiO_2. As we have recently reported,[15−18] additional information is possible, such as phase matchability (Type I) and an estimation of the average NLO susceptibility, $\langle d_{ijk}^{2\omega}\rangle$ or $\langle d_{\text{eff}}\rangle$. Before continuing, more detail regarding phase matching and $\langle d_{ijk}^{2\omega}\rangle$ is required. To maximize the SHG intensity, geometries are sought that match wave vectors and thereby match the phases of the fundamental and harmonic beams. Type I phase-matching, also called index matching, occurs when the phase velocity of the fundamental frequency is equal to the phase velocity of the harmonic radiation. Type II phase-matching occurs when an extraordinary, or ordinary, ray at the harmonic frequency is produced by a combination of one ordinary and one extraordinary ray at the fundamental frequency. In a powder SHG experiment, the ordinary and extraordinary rays are not separated; thus, only Type I phase-matching can be investigated. (There are two other types of phase-matching, critical and noncritical, but these can only be investigated through single-crystal SHG experiments and will not be discussed here.)

Experimentally, Type I phase-matching is determined by measuring the SHG intensity as a function of particle size. If the material is Type I phase-matchable, the SHG intensity will increase with particle size and plateau at a maximum value. If the material is *not* Type I phase-matchable, the SHG intensity will reach a maximum and then decrease with increasing particle size. Once the Type I phase-matching capabilities of a material are known, one can determine the average NLO susceptibility, $\langle d_{ijk}^{2\omega}\rangle$. If the material in question is not phase-matchable (NPM), the SHG intensity ratio is[15,27]

$$\frac{I^{2\omega}(\text{A})}{I^{2\omega}(\text{SiO}_2)} = \frac{\langle d(\text{A})_{ijk}^{2\omega}\rangle^2 (l_c^2/2r)(\text{A})}{\langle d(\text{SiO}_2)_{ijk}^{2\omega}\rangle^2 (l_c^2/2r)(\text{SiO}_2)} \qquad (1)$$

For SiO_2, the coherence length, l_c, is 20 μm, the average particle size, r, is 50 μm, and $\langle d(\text{SiO}_2)_{ijk}^{2\omega}\rangle^2 = 7.62 \times 10^{-2}$ pm^2/V^2.[28,29] For all other NPM materials, l_c and r are assumed to be 10 and 50 μm, respectively. Equation 1 simplifies to

$$\frac{I^{2\omega}(\text{A})}{I^{2\omega}(\text{SiO}_2)} = \frac{\langle d(\text{A})_{ijk}^{2\omega}\rangle^2}{0.3048} \qquad (2)$$

Thus, for a NPM material, if the SHG intensity ratio with respect to SiO_2 has been measured, for a particular particle size range (45−63 μm is often used), $\langle d_{ijk}^{2\omega}\rangle$ can be calculated. If the material in question is phase-matchable (PM), the SHG intensity ratio simplifies to[15,27]

$$\frac{I^{2\omega}(\text{A})}{I^{2\omega}(\text{LiNbO}_3)} = \frac{\langle d(\text{A})_{ijk}^{2\omega}\rangle^2}{\langle d(\text{LiNbO}_3)_{ijk}^{2\omega}\rangle^2} \qquad (3)$$

where $\langle d(\text{LiNbO}_3)_{ijk}^{2\omega}\rangle^2 = 7.98 \times 10^2$ pm^2/V^2.[29] Similar to the NPM case, once the SHG intensity ratio is known, $\langle d(\text{A})_{ijk}^{2\omega}\rangle$ can be calculated. One very important caveat, because the SHG intensity will vary as the particle size changes, it is imperative that a specific particle size range, for example, 45−63 μm, is used to compare SHG intensities. SHG intensity comparisons on ungraded samples should be regarded with great caution and may be in error by as much as a factor of 5.

Experimental Section

Reagents. TeO_2 (99% Aldrich), WO_3 (99% Aldrich), Na_2CO_3 (99.5% Alfa Aesar), and NaOH (98%, EM Science) were used as received.

Syntheses. Single crystals of $Na_2TeW_2O_9$ were initially prepared hydrothermally from a solution of 3 M NaOH, WO_3, and TeO_2. The oxides, 0.1788 g of WO_3 (7.711×10^{-4} mol) and 0.0273 g of TeO_2 (1.714×10^{-4} mol), were combined with 0.2570 mL of 3.0 M (7.711×10^{-4} mol) NaOH in a gold tube. The gold tube (i.d. = 6.1 mm, o.d. = 4.9 mm, and length = 44.0 mm) was welded closed and placed into a LECO autoclave. The autoclave was filled with 18 mL (60% fill) of H_2O, sealed, and heated to 470 °C. At 470 °C an autogenous pressure of 6750 psi (459 atm) was observed. After 48 h at 470 °C the autoclave was cooled slowly (6 °C h^{-1}) to room temperature. The gold tubes were retrieved from the autoclave and opened. A single-phase product of cream-colored columnar crystals was recovered in 65% yield based on TeO_2, by filtration.

Polycrystalline $Na_2TeW_2O_9$ was obtained by standard solid-state methods. Stoichiometric amounts of Na_2CO_3, TeO_2, and WO_3 were ground and pressed into pellets that were heated in air to 450 °C for 12 h and then to 650 °C for 3 days with three intermittent re-grindings. Powder X-ray diffraction patterns of the bulk polycrystalline phases are in good agreement with a calculated pattern derived from the single-crystal data (see Supporting Information).

Crystallographic Determination. The structure of $Na_2TeW_2O_9$ was determined by standard crystallographic methods. A cream-colored column (0.03 × 0.10 × 0.20 mm) was used for single-crystal measurements. Room-temperature intensity data were collected on a Siemens SMART diffractometer equipped with a 1 K CCD area detector using graphite monochromated Mo Kα radiation. A hemisphere of data was collected using a narrow-frame method with scan widths of 0.30° in ω and an exposure time of 25 s/frame. The first 50 frames were remeasured at the end of the data collection to monitor instrument and crystal stability. The maximum correction applied to the intensities was <1%. The data were integrated using the Siemens SAINT program,[30] with the

(24) Balraj, V.; Vidyasagar, K. *Inorg. Chem.* **1999**, *38*, 5809.
(25) Balraj, V.; Vidyasagar, K. *Inorg. Chem.* **1999**, *38*, 1394.
(26) Balraj, V.; Vidyasagar, K. *Inorg. Chem.* **1999**, *38*, 3458.
(27) Kurtz, S. K.; Perry, T. T. *J. Appl. Phys.* **1968**, *39*, 3798.
(28) Miller, R. C. *Appl. Phys. Lett.* **1964**, *5*, 17.
(29) Jerphagnon, J.; Kurtz, S. K. *Phys. Rev.* **1970**, *1B*, 1738.
(30) *SAINT*, Version 4.05 ed.; Siemens Analytical X-ray Systems, Inc.: Madison, WI, 1995.

Table 1. Crystallographic Data for $Na_2TeW_2O_9$

empirical formula	Na2 O9 Te W2
formula weight	685.28
temperature (K)	293.0(2)
wavelength (Å)	0.71073
crystal system, space group	monoclinic, *Ia* (No. 9, cell choice 3)
unit cell dimensions (Å)	$a = 13.1394(5)$ $b = 7.3202(3)$ $\beta = 95.0270(10)°$ $c = 31.4435(11)$
volume (Å^3)	3012.7(2)
Z	16
ρ (g/cm^3)	6.043
μ (cm^{-1})	344.59
crystal size	0.03 × 0.10 × 0.20 mm
reflections collected/unique	9345/4964 [R(int) = 0.0380]
refinement method	full-matrix least-squares on F^2
goodness-of-fit on F^2	0.931
absolute structure parameter	0.19(2)
$R(F)^a$	0.0331
$R_w(F)^b$	0.0986

^{a} $R = \Sigma\,||F_o| - |F_c||/\Sigma\,|F_o|$. ^{b} $R_w = [\Sigma w(|F_o|^2 - |F_c|^2)^2/\Sigma w(F_o^2)^2]^{1/2}$.

intensities corrected for Lorentz, polarization, air absorption, and absorption attributable to the variation in path length through the detector faceplate. ψ scans were used for the absorption correction on the hemisphere of data. The data were solved and refined using SHELXS-97 and SHELXL-97, respectively.[31,32] The tungsten and tellurium atoms were refined with anisotropic thermal parameters, and all oxygen atoms were refined isotropically. The data converged for $I > 2\sigma(I)$. All calculations were performed using the WinGX-98 crystallographic software package.[33] Crystallographic data, atomic coordinates and thermal parameters, and selected bond distances are listed in Tables 1−3.

Infrared Spectroscopy. Infrared spectra were recorded on a Matteson FTIR 5000 spectrometer in the 400−4000-cm^{-1} range, with the sample pressed between two KBr pellets.

Thermogravimetric Analysis. Thermogravimetric analyses were carried out on a TGA 2950 thermogravimetric analyzer (TA instruments). The sample was contained within a platinum crucible and heated in air at a rate of 5 °C min^{-1} to 950 °C.

Second-Order Nonlinear Optical Measurements. Powder SHG measurements were performed on a modified Kurtz-NLO[27] system using 1064-nm radiation. A detailed description of the equipment and the methodology used have been published.[15,17] No index-matching fluid was used in any of the experiments. Powders with particle sizes of 45−63 μm were used for comparing SHG intensities.

Results and Discussion

The major building block of the new noncentrosymmetric tellurite $Na_2TeW_2O_9$ are corrugated layers of corner-sharing WO_6 octahedra (see Scheme 1). Three-coordinate tellurium atoms link the two-dimensional tungsten oxide network forming the three-dimensional structure (see Figure 1a,b). The numerous small cavities found within the Te−W−O network are occupied by Na^+ ions, which maintain charge neutrality. The connectivity of the tungsten oxide layers, which stack along [100], is shown in Figure 2. There are eight crystallographically unique tungsten atoms in $Na_2TeW_2O_9$. Each is octahedrally coordinated by oxygen with W−O bond lengths ranging from 1.711(15) Å − 2.251(15) Å. All of the WO_6 octahedra are distorted with three short and three long W−O bonds. The most distorted octahedral environment occurs with W3, which has one O−W−O angle of 71.4(5)° and bond distances ranging from 1.759(14) to 2.177(13) Å. The calculated bond valence values[34,35] for W^{6+} range from 5.94 to 6.30. All the tungsten octahedra in the two-dimensional $W_8O_{36}^{24-}$ block are corner-shared with at least two other WO_6 units. The corrugated layers are built up from two $W_4O_{18}^{12-}$ units that run parallel to the [001] direction. The W1−W3−W5−W7- and W8−W6−W4−W2-based octahedra are

Table 2. Atomic Coordinates for $Na_2TeW_2O_9$

atom	x	y	z	$U_{(eq)}{}^a$ (Å^2)
Na1	0.2672(10)	0.2378(12)	0.5033(5)	0.028(3)
Na2	0.4235(7)	0.4897(10)	0.8029(3)	0.016(2)
Na3	0.0275(7)	0.5172(13)	0.4989(3)	0.019(2)
Na4	0.2041(6)	0.5066(10)	0.5962(3)	0.0105(17)
Na5	0.5596(10)	0.4863(12)	0.6914(4)	0.032(3)
Na6	0.3011(12)	0.7417(11)	0.6948(5)	0.028(2)
Na7	0.5538(9)	0.9858(13)	0.7011(4)	0.0285(17)
Na8	0.3007(8)	1.0225(14)	0.4002(4)	0.0285(17)
Te1	0.41444(12)	−0.00312(15)	0.78898(5)	0.0086(2)
Te2	0.00518(11)	0.01726(15)	0.49667(4)	0.0080(2)
Te3	0.30205(10)	0.53021(16)	0.41396(4)	0.0098(2)
Te4	0.20097(12)	1.00755(14)	0.60672(5)	0.0079(2)
W1	0.44469(5)	0.73831(9)	0.60799(3)	0.00715(18)
W2	0.44203(6)	0.25205(9)	0.59726(3)	0.00687(18)
W3	0.28125(6)	0.74136(9)	0.50170(3)	0.00735(17)
W4	0.30579(7)	0.27708(9)	0.69683(3)	0.00895(16)
W5	0.06938(6)	0.78029(9)	0.40053(3)	0.00696(16)
W6	0.15682(6)	0.25635(9)	0.79220(3)	0.00682(17)
W7	0.15686(6)	0.74465(9)	0.78810(3)	0.00777(18)
W8	0.06307(6)	0.27122(9)	0.40377(3)	0.00687(16)
O1	0.5616(11)	0.6863(18)	0.5911(5)	0.018(3)^b
O2	0.4666(11)	0.7367(16)	0.6641(5)	0.014(3)
O3	0.3895(12)	0.4942(17)	0.6031(5)	0.015(3)
O4	0.4623(12)	0.9966(17)	0.6002(5)	0.015(3)
O5	0.3902(12)	0.7398(16)	0.5410(5)	0.013(3)
O6	0.2898(11)	0.8100(19)	0.6120(5)	0.017(3)
O7	0.4467(12)	0.2687(18)	0.5426(5)	0.019(3)
O8	0.5677(11)	0.3012(19)	0.6187(5)	0.018(3)
O9	0.2856(10)	0.1896(18)	0.5876(4)	0.012(3)
O10	0.4045(10)	0.2252(15)	0.6622(4)	0.010(3)
O11	0.2066(10)	0.9284(17)	0.5163(4)	0.014(3)
O12	0.2080(11)	0.5603(18)	0.5196(5)	0.015(3)
O13	0.2209(12)	0.7224(18)	0.4371(5)	0.017(3)
O14	0.3696(10)	0.5413(16)	0.4695(4)	0.011(2)
O15	0.3716(10)	0.9494(17)	0.4727(4)	0.011(2)
O16	0.2320(11)	0.4365(18)	0.6668(5)	0.017(3)
O17	0.3762(10)	0.4274(18)	0.7321(5)	0.017(3)
O18	0.3524(11)	0.0379(18)	0.7346(5)	0.018(3)
O19	0.1842(12)	0.2731(17)	0.7376(5)	0.016(3)
O20	0.2102(9)	0.0614(16)	0.6653(4)	0.010(2)
O21	−0.0521(11)	0.818(2)	0.3755(5)	0.019(3)
O22	0.1436(11)	0.7134(18)	0.3573(5)	0.015(3)
O23	0.1168(9)	1.0179(14)	0.4021(4)	0.001(2)
O24	0.0428(10)	0.5183(15)	0.4159(4)	0.008(2)
O25	0.0296(9)	0.8171(16)	0.4605(4)	0.009(2)
O26	0.2781(12)	0.298(2)	0.8179(5)	0.020(3)
O27	0.1766(11)	0.0010(16)	0.7920(5)	0.012(3)
O28	0.1047(11)	0.4968(17)	0.7987(5)	0.013(3)
O29	0.0968(11)	0.1991(19)	0.8510(5)	0.019(3)
O30	0.0015(10)	0.1880(17)	0.7718(4)	0.013(2)
O31	0.2828(11)	0.690(2)	0.8019(5)	0.020(3)
O32	0.1470(13)	0.7352(18)	0.7315(6)	0.022(4)
O33	0.0009(11)	0.8030(19)	0.7888(5)	0.016(3)
O34	−0.0621(11)	0.2060(18)	0.3935(4)	0.013(3)
O35	0.0665(11)	0.2174(17)	0.4674(5)	0.015(3)
O36	0.2254(10)	0.3244(17)	0.4254(4)	0.012(2)

^{a} $U_{(eq)}$ is defined as one-third of the trace of the orthogonalized $\mathbf{U}_{ij}$ tensor. ^{b} All oxygen atoms were refined isotropically.

(31) Sheldrick, G. M. *SHELXS-97 - A program for automatic solution of crystal structures*; University of Göttingen: Göttingen, Germany, 1997.
(32) Sheldrick, G. M., *SHELXL-97 - A program for crystal structure refinement*; University of Göttingen: Göttingen, Germany, 1997.
(33) Farrugia, L. J. *J. Appl. Crystallogr.* **1998**, *32*, 837.
(34) Brown, I. D.; Altermatt, D. *Acta Crystallogr.* **1985**, *B41*, 244.
(35) Brese, N. E.; O'Keeffe, M. *Acta Crystallogr.* **1991**, *B47*, 192.

Scheme 1

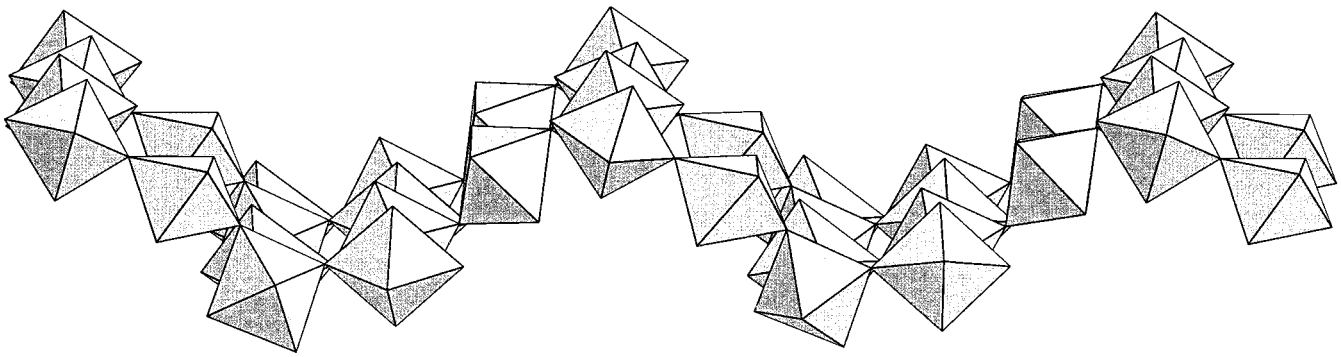

Table 3. Selected Bond Distances (Å) for $Na_2TeW_2O_9$[a]

W(1)−O(1)	1.712(14)	W(2)−O(3)	1.917(13)
W(1)−O(2)	1.763(15)	W(2)−O(4)#1	1.890(13)
W(1)−O(3)	1.929(13)	W(2)−O(7)	1.729(17)
W(1)−O(4)	1.923(13)	W(2)−O(8)	1.765(15)
W(1)−O(5)	2.166(15)	W(2)−O(9)	2.101(13)
W(1)−O(6)	2.117(15)	W(2)−O(10)	2.150(14)
W(3)−O(5)	1.807(15)	W(4)−O(10)	1.806(14)
W(3)−O(11)	1.768(13)	W(4)−O(16)	1.741(14)
W(3)−O(12)	1.759(14)	W(4)−O(17)	1.766(14)
W(3)−O(13)	2.118(15)	W(4)−O(18)	2.173(14)
W(3)−O(14)	2.174(13)	W(4)−O(19)	2.135(16)
W(3)−O(15)	2.179(13)	W(4)−O(20)	2.199(12)
W(5)−O(13)	2.250(15)	W(6)−O(19)	1.788(16)
W(5)−O(21)	1.738(14)	W(6)−O(26)	1.750(15)
W(5)−O(22)	1.809(15)	W(6)−O(27)	1.887(12)
W(5)−O(23)	1.847(11)	W(6)−O(28)	1.906(13)
W(5)−O(24)	2.016(12)	W(6)−O(29)	2.116(15)
W(5)−O(25)	2.019(12)	W(6)−O(30)	2.145(13)
W(7)−O(22)#4	2.220(15)	W(8)−O(23)#1	1.987(10)
W(7)−O(27)#6	1.897(12)	W(8)−O(24)	1.873(12)
W(7)−O(28)	1.977(13)	W(8)−O(29)#7	1.767(15)
W(7)−O(31)	1.720(14)	W(8)−O(34)	1.715(14)
W(7)−O(32)	1.774(18)	W(8)−O(35)	2.036(15)
W(7)−O(33)	2.096(14)	W(8)−O(36)	2.215(13)
Te(1)−O(18)	1.854(15)	Te(2)−O(15)#5	1.864(13)
Te(1)−O(30)#2	1.881(13)	Te(2)−O(25)#1	1.899(12)
Te(1)−O(33)#3	1.854(14)	Te(2)−O(35)	1.942(14)
Te(3)−O(13)	1.946(14)	Te(4)−O(6)	1.856(14)
Te(3)−O(14)	1.890(13)	Te(4)−O(9)#6	1.869(13)
Te(3)−O(36)	1.865(13)	Te(4)−O(20)#6	1.878(13)

[a] Symmetry transformations used to generate equivalent atoms: (#1) $x, y - 1, z$; (#2) $x + 1/2, -y, z$; (#3) $x + 1/2, -y + 1, z$; (#4) $x, -y + 3/2, z + 1/2$; (#5) $x - 1/2, -y + 1, z$; (#6) x, y + 1, z; (#7) $x, -y + 1/2, z - 1/2$.

connected in a trans−trans−cis and trans−trans−trans fashion, respectively (see Figure 2). The $W_4O_{18}^{12-}$ moieties are connected to one another along the *b* axis, in a trans fashion, through the W8−W5-, W6−W7-, and W2−W1-based octahedra. Small cavities (diameter ∼ 4.8 Å) form next to the W3- and W4-based octahedra, which are not connected to any other WO_6 units along the direction of the *b* axis. All of the WO_6 octahedra are skewed with respect to each other attributable to the distorted environment of each individual W atom.

The positions of the four crystallographically unique tellurium atoms found in $Na_2TeW_2O_9$ are highlighted in Figure 3. All tellurium atoms are three-coordinate with Te−O bond lengths ranging from 1.852(14) to 1.944(15) Å. The calculated bond valence values[34,35] for Te^{4+} range from 3.70 to 4.09. The tellurium atoms are each connected to the oxygen atoms of three different WO_6 octahedra. This type of TeO_3 connectivity, pyramidal $[TeO_{3/2}]^+$, is common in tellurites.[23−26,36] The distorted trigonal pyramidal geometry formed by these interactions is typical of three-coordinate Te^{4+}, which has a nonbonding lone pair of electrons. The Te3 and Te4 atoms cap the $W_8O_{36}^{24-}$ layers from above and below. The Te1 and Te2 atoms connect adjacent tungsten oxide layers, completing the $Te_4W_8O_{36}^{8-}$ three-dimensional anionic network.

Within the three-dimensional Te−W−O anionic unit there are narrow channels and cavities. These small spaces, <4 Å in diameter, are occupied by the lone pairs on the Te^{4+} atoms and charge-compensating Na^+ ions. There are eight crystallographically independent Na atoms found in $Na_2TeW_2O_9$. The closest Na−O, Na−W, Na−Te, and Na−Na distances are 2.239(16), 3.405(8), 3.450(13), and 3.580(18) Å, respectively.

Infrared Spectroscopy. The infrared spectra of $Na_2TeW_2O_9$ reveals a series of W−O, Te−O, and W−O−Te vibrations found in the region between 600 and 950 cm^{-1}. The stretches between 770 and 950 cm^{-1} can be attributed to the W−O vibrations.[24] The stretches between 600 and 950 cm^{-1} represent a combination of the W−O, Te−O, and W−O−Te vibrations.[37−39]

Thermogravimetric Analysis. The thermal behavior of $Na_2TeW_2O_9$ was investigated using thermogravimetric analysis. A single-step decomposition indicates $Na_2TeW_2O_9$ volatilizes above 800 °C.

Second-Order Nonlinear Optical Measurements. Second-harmonic-generating (SHG) measurements on sieved $Na_2TeW_2O_9$ indicate the material is phase-matchable (Type I) (see Figure 4) with an intensity of approximately 500× SiO_2. The SHG efficiency of $Na_2TeW_2O_9$ compares favorably with respect to $LiNbO_3$ (600× SiO_2) and $BaTiO_3$ (400× SiO_2). As we stated in the background section, once the phase-matching behavior and SHG intensity are known, the average NLO susceptibility, $\langle d_{ijk}^{2\omega} \rangle$, can be calculated. For phase-matchable materials:

$$\langle d_{ijk}^{2\omega} \rangle = \left[7.98 \times 10^2 \left(\frac{I_{Na_2TeW_2O_9}^{2\omega}}{I_{LiNbO_3}^{2\omega}} \right) \right]^{1/2}$$

where $I_{LiNbO_3}^{2\omega}$ is the SHG intensity of $LiNbO_3$ compared

(36) Feger, C. R.; Kolis, J. W. *Inorg. Chem.* **1998**, *37*, 4046.
(37) Szaller, Z.; Kovacs, L.; Poppl, L. J. *J. Solid State Chem.* **2000**, *152*, 392.
(38) Dimetriev, Y.; Bart, J. C. J.; Dimitrov, V.; Arnaudov, M. *Z. Anorg. Allg. Chem.* **1981**, *479*, 229.
(39) Arnaudov, M.; Dimitrov, V.; Dimitriev, Y.; Markova, L. *Mater. Res. Bull.* **1982**, *17*, 1121.

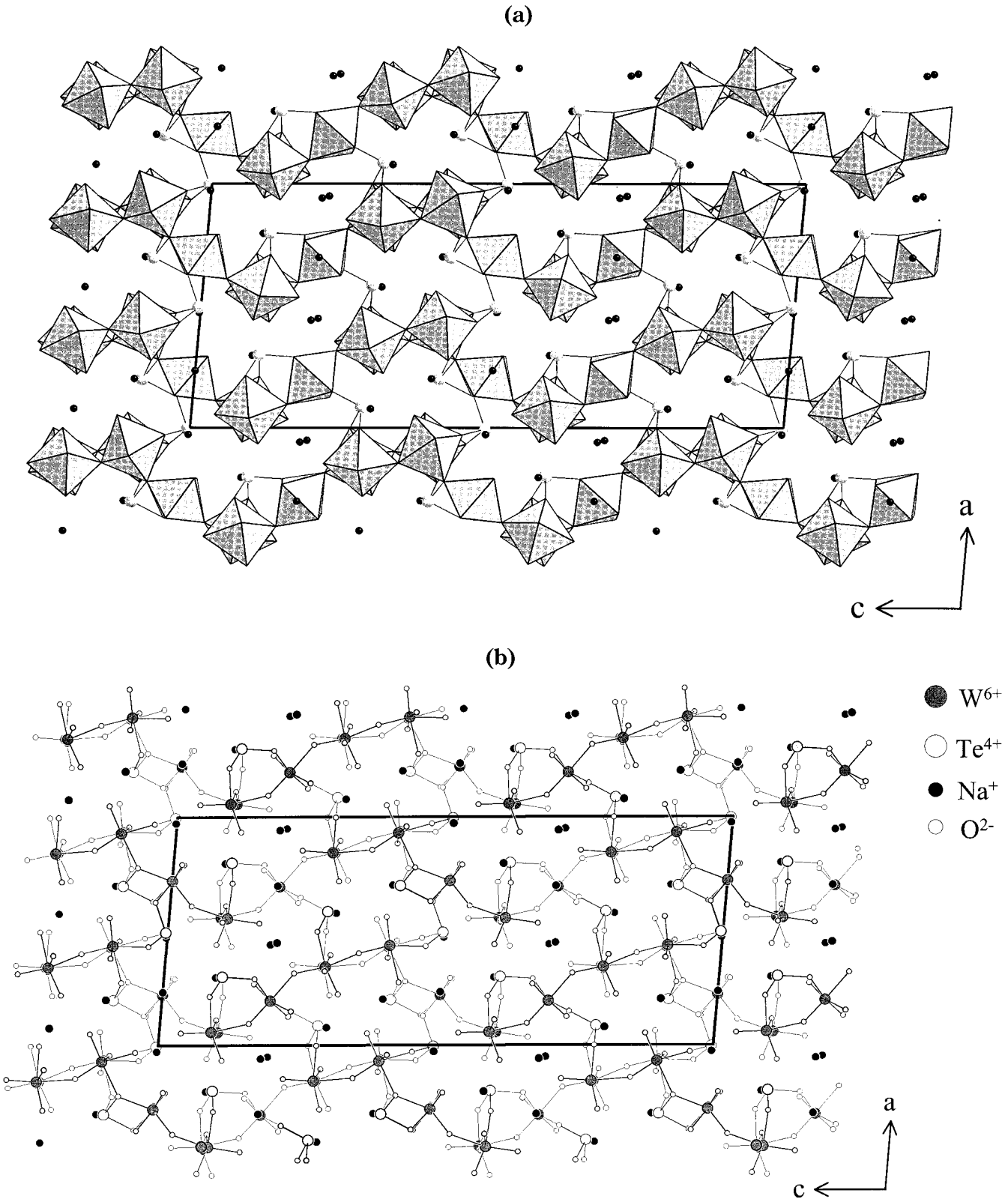

Figure 1. Polyhedral (a) and ball-and-stick (b) representations of $Na_2TeW_2O_9$ viewed down the [010] direction. In (a) the shaded polyhedra represent $W^{6+}O_6$ octahedra, the gray spheres represent Te^{4+} atoms, and the small black spheres represent Na^+ ions.

to SiO_2. Because $I^{2\omega}_{LiNbO_3} = 600$ and $I^{2\omega}_{Na_2TeW_2O_9} = 500$, $\langle d^{2\omega}_{ijk} \rangle = 26$ pm/V.

One of our motivations in studying SHG materials is to elucidate the structure origin of the magnitude of the SHG response. One requirement for a large SHG response is that the individual bond hyperpolarizabilities (β's) should "constructively add".[19−22] That is, to maximize the SHG response, the polarizations attributable to the individual M−O bonds should be aligned in the structure. The magnitude of the SHG response is directly dependent on the orientation and magnitude of β(M−O). Thus, if the individual β's for a given material are known, it should be possible to calculate the magnitude of the SHG response. This method was

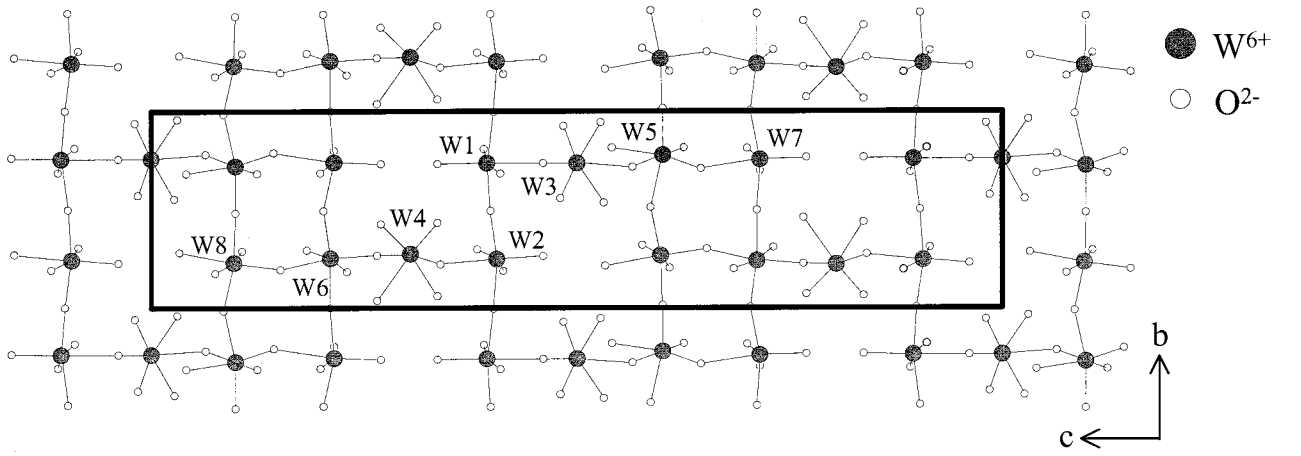

Figure 2. An *a*-axis view of the corner-sharing $W_8O_{36}^{24-}$ layer in $Na_2TeW_2O_9$ is shown. The eight crystallographically unique W atoms are highlighted.

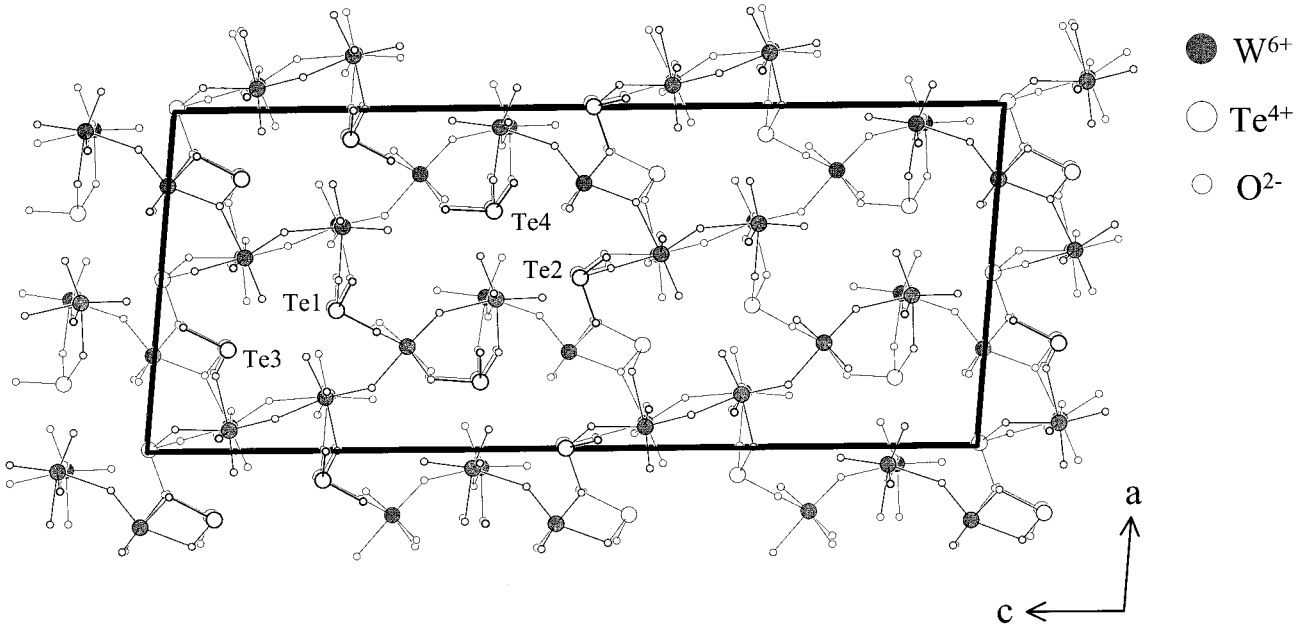

Figure 3. A *b*-axis view of the anionic $Te_4W_8O_{36}^{8-}$ unit in $Na_2TeW_2O_9$ is shown. The Te3 and Te4 cap the tungsten oxide layers while Te1 and Te2 connect adjacent layers.

first suggested some time ago[22] and utilizes a direction cosine approach with respect to the M−O bonds, where the *i*th M−O bond has direction cosines l_i, m_i, and n_i, from the positive atom to the more electronegative atom. In essence, the model fundamentally relates the individual NLO coefficients, d_{ijk}, with the bond hyperpolarizability, β. For example, $d_{123} = l_i m_i n_i \beta(\text{M}-\text{O})$ and $d_{333} = n_i^3 \beta(\text{M}-\text{O})$. Once the individual NLO coefficients, d_{ijk}'s, are known, one can then calculate the average NLO susceptibility, $\langle d_{ijk}^{2\omega} \rangle$, for the material. For cations with nonbonded electron pairs, for example, Te^{4+}, the lone pair is assumed to have a similar β to that of the metal oxygen bond.[40]

In their original paper, Kurtz and Perry deduced that for unpolarized fundamental and second-harmonic light[27]

$$\langle d_{ijk}^{2\omega} \rangle^2 = (19/105)\Sigma_i (d_{iii})^2 + (13/105)\Sigma_{i \neq j} (d_{iii})(d_{ijj}) + (44/105)\Sigma_{i \neq j} (d_{iij})^2 + (13/105)\Sigma_{ijk,\text{cyclic}} (d_{iij})(d_{jkk}) + (5/7)(d_{ijk})^2 \quad (4)$$

$Na_2TeW_2O_9$ crystallizes in space group *Ia* that is in

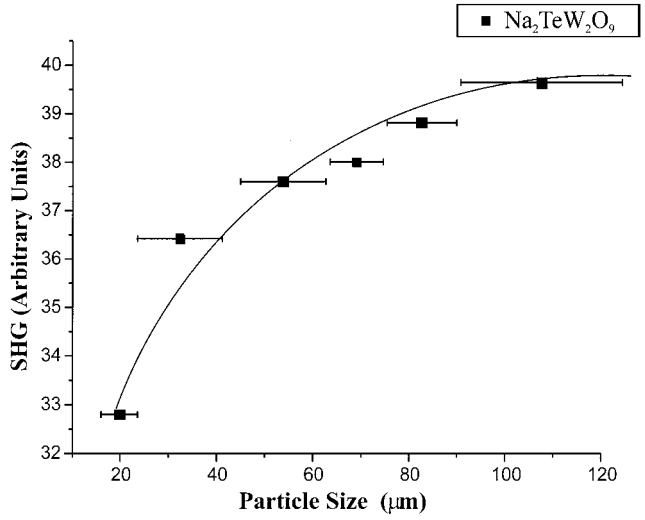

Figure 4. Phase-matching curve, that is, particle size vs SHG intensity, for $Na_2TeW_2O_9$ is given. The curve drawn is to guide the eye and is not a fit to the data.

crystal class *m*. For crystal class *m*, eq 4 reduces to

$$\langle d_{ijk}^{2\omega}\rangle^2 = (19/105)[(d_{111})^2 + (d_{333})^2] + (13/105)[(d_{111})(d_{122}) + (d_{111})(d_{133}) + (d_{333})(d_{311}) + (d_{333})(d_{322})] + (44/105)[(d_{113})^2 + (d_{223})^2 + (d_{331})^2] + (13/105)[(d_{113})(d_{322}) + (d_{223})(d_{311}) + (d_{331})(d_{122})] \quad (5)$$

where Kleinman symmetry is assumed.[41] For $Na_2TeW_2O_9$, two types of bond hyperpolarizabilies exist, $\beta(W^{6+}-O)$ and $\beta(Te^{4+}-O)$. From previous work, $\beta(W^{6+}-O)$ has been calculated to be $570 \pm 130 \times 10^{-40}$ m^4/V (100 ± 23 pm/V),[42,43] whereas we estimate $\beta(Te^{4+}-O)$ to be 130×10^{-40} m^4/V (22.9 pm/V) based on powder SHG measurements of Te_2SeO_7.[15] Thus, individual d_{ijk}'s can be calculated from both $\beta(W^{6+}-O)$ and $\beta(Te^{4+}-O)$, and inserting these β values into eq 5 allows us to estimate $\langle d_{ijk}^{2\omega}\rangle$. For $Na_2TeW_2O_9$, we estimate a value for $\langle d_{ijk}^{2\omega}\rangle$ of 100 ± 20 pm/V. The calculated value is larger than our measured value of 26 pm/V, suggesting that the magnitude of the SHG intensity is not entirely attributable to a vectoral addition of the individual bond hyperpolarizabilities and is attenuated by other factors. The discrepancy between calculated and measured $\langle d_{ijk}^{2\omega}\rangle$ values also suggests the estimation of $\beta(W^{6+}-O)$ and $\beta(Te^{4+}-O)$ may be too large.

One of the interesting aspects of the model is that the methodology can be used "in reverse". That is, once $\langle d_{ijk}^{2\omega}\rangle$ has been measured, through powder SHG experiments, β(M−O) can be estimated for a variety of metals. Because the individual d_{ijk}'s are related to β(M−O) through the direction cosines, one simply substitutes β(M−O) (with the appropriate direction cosines) into eq 5 and solves for β(M−O). We have measured the powder SHG efficiency for a number of materials to estimate β(M−O) values for a variety of metal cations. The values for β(M−O) and the compounds used in the experiments are given in Table 4. For completion, we have also included the values for β(M−O) for some metals from the original paper of Bergman and Crane.[22] We are continuing to collect powder SHG data, in order to further refine the β's in Table 4.

Table 4. β(M−O) for Various Metals

M−O	$\beta \times 10^{-40}$ (m^4/V)	compound
$Ti^{4+}-O$	495	$BaTiO_3$[44]
$Nb^{5+}-O$	240	$LiNbO_3$[45]
$Ta^{5+}-O$	200	$LiTaO_3$[46]
$Mo^{6+}-O$	305	$RbMoO_3(IO_3)$[47]
$W^{6+}-O$	570 ± 130[42]	$Li_{1-x}(Nb,Ta)_{1-x}W_xO_3$[42]
$Te^{4+}-O$	130	Te_2SeO_7[15]
$Se^{4+}-O$	160	$TeSeO_4$[14]
$Pb^{2+}-O$	865	$PbTiO_3$[48]
$N^{3+}-O$	12[22]	$NaNO_2$[49]
$P^{5+}-O$	17[22]	KH_2PO_4[50]
$Cl^{5+}-O$	11[22]	$NaClO_3$[51]
$Br^{5+}-O$	23[22]	$NaBrO_3$[51]
$I^{5+}-O$	140	$LiIO_3$,[52] HIO_3[53]

Summary

The combination of SOJT distorted cations, specifically W^{6+} and Te^{4+}, has resulted in the creation of a new NCS compound, $Na_2TeW_2O_9$. The material contains two asymmetrically coordinated metal cations. The asymmetric coordination of both W^{6+} and Te^{4+} produces local polarizations that "constructively add", resulting in a large (500× quartz) SHG response. We are in the process of synthesizing other W^{6+}/Te^{4+} NCS oxides and will be reporting on them shortly.

Acknowledgment. We acknowledge Dr. James Korp for technical assistance with the crystallography. We thank the Robert A. Welch Foundation for support. This work used the MRSEC/TCSUH Shared Experimental Facilities supported by the National Science Foundation under Award DMR-9632667 and the Texas Center for Superconductivity at the University of Houston. This work was also supported by the NSF-Career Program through DMR-0092054 and an acknowledgment is made to the donors of the Petroleum Research Fund, administered by the American Chemical Society, for partial support of this research. PSH is a Beckman Young Investigator.

Supporting Information Available: Powder X-ray diffraction patterns (calculated and experimental) (PDF) and X-ray crystallographic data are available (CIF). This material is available free of charge via the Internet at http://pubs.acs.org.

CM020087I

(40) Bergman, J. G.; Crane, G. R. *J. Chem. Phys.* **1974**, *60*, 2470.
(41) Kleinman, D. A. *Phys. Rev.* **1962**, *126*, 1977.
(42) Wiegel, M.; Emond, M. H. J.; de Bruin, T. H. M.; Blasse, G. *Chem. Mater.* **1994**, *6*, 973.
(43) Unit Conversion: 1 pm/V = 2.387×10^{-9} esu and 1×10^{-40} m^4/V = 4.189×10^{-10} esu. NLO susceptibility: $\langle d_{ijk}^{2\omega}\rangle$ (pm/V) $\xrightarrow{5.698\times10^{-40}}$ $\beta \times 10^{-40}$ (m^4/V). Molecular hyperpolarizability: $\beta \times 10^{-40}$ (m^4/V) $\xrightarrow{1.755\times10^{-40}}$ $\langle d_{ijk}^{2\omega}\rangle$ (pm/V).
(44) Shirane, G.; Danner, H.; Pepinsky, R. *Phys. Rev.* **1957**, *105*, 846.
(45) Abrahams, S. C.; Reddy, J. M.; Bernstein, J. L. *J. Phys. Chem. Solids* **1966**, *27*, 997.
(46) Abrahams, S. C.; Bernstein, J. L. *J. Phys. Chem. Solids* **1967**, *28*, 1685.
(47) Sykora, R. E.; Ok, K. M.; Halasyamani, P. S.; Runde, W.; Albrecht-Schmitt, T. E. *J. Am. Chem. Soc.* **2002**, *1951*, 124.
(48) Shirane, G.; Pepinsky, R.; Frazer, B. C. *Phys. Rev.* **1955**, *97*, 1179.
(49) Kay, M. I.; Frazer, B. C. *Acta Crystallogr.* **1961**, *14*, 56.
(50) Bacon, G. E.; Pease, R. S. *Proc. R. Soc. London, A* **1955**, *230*, 359.
(51) Abrahams, S. C.; Bernstein, J. L. *Acta Crystallogr.* **1977**, *B33*, 3601.
(52) Svensson, C.; Albertsson, J.; Liminga, R.; Kvick, A.; Abrahams, S. C. *J. Chem. Phys.* **1983**, *78*, 7343.
(53) Stahl, K.; Szafransk, M. *Acta Crystallogr.* **1992**, *C48*, 1571.